

# Cancellation of periodic disturbances for dual start induction drives based on a novel robust adaptive control strategy

Ngoc Thuy Pham, Phu Diep Nguyen

Department of Electrical Engineering Technology, Industrial University of Ho Chi Minh City, Ho Chi Minh, Vietnam

## Article Info

### Article history:

Received Sep 24, 2024

Revised May 12, 2025

Accepted May 25, 2025

### Keywords:

Disturbance cancellation  
Dual start induction motor  
FOC vector control  
High-order sliding mode  
Repetitive control

## ABSTRACT

The disturbance cancellation has always been an important area that has received much attention, especially for the nonlinear drive systems as the dual start induction motor (DSIM). In this paper, a new robust adaptive hybrid strategy based on an improved variable-gain quasi-continuous third-order sliding mode (VGQSTOSM) algorithm integrated with RC and a load torque disturbance estimator helps to reduce chattering, cancel the periodic and extended load disturbances, and enhance tracking performance effectively. By using third-order sliding mode with variable gain dependent on the magnitude of the sliding variable, this proposal aims to be adaptive. It provides higher gain when far from the sliding surface (is large), leading to faster convergence and lower gain when close to the sliding surface (is small), potentially reducing chattering further and decreasing control effort near the equilibrium. The robustness of the proposed controller is improved because the adaptive gain mechanism effectively compensates for uncertainties or disturbances. Furthermore, a plug-in RC is integrated into the improved high-order sliding mode structure (DRVGQSTOSM), and an estimated load torque disturbance value is also used to help identify and proactively eliminate disturbances. The system stability is assured using Lyapunov theory the virtual control vectors' outputs are chosen based on Lyapunov theory. Simulation results obtained using the MATLAB software confirm the tracking and harmonic disturbance rejection performance as well as the robustness of the proposed control strategy.

This is an open access article under the [CC BY-SA](#) license.



## Corresponding Author:

Ngoc Thuy Pham

Department of Electrical Engineering Technology, Industrial University of Ho Chi Minh City

Ho Chi Minh, Vietnam

Email: phamthuyngoc@iuh.edu.vn, ngocpham1020@gmail.com

## 1. INTRODUCTION

The dual start induction motor (DSIM) drives are one of the multiphase motor drives that have garnered significant research attention in recent decades. They are increasingly employed in high-power industrial applications demanding high-quality control, reliability, and fault tolerance. Their application is particularly notable in the transportation sector, including electric vehicles (EVs), ships, and aeronautics. DSIMs are progressively replacing traditional three-phase induction motors in AC drives where high reliability, accuracy, safety, and fault tolerance are paramount [1]-[3]. Despite the outstanding advantages, DSIM has its inherent problems of nonlinearity and coupling, which are challenges for control systems design. Additionally, the external disturbances, such as sudden load changes, periodic disturbances, also decrease the performance of the drives.

To address these challenges, advanced control methods based on modern vector control strategies have been developed for DSIM drives. In that, direct torque control (DTC) stands out as a relatively simple

strategy. Its advantages include fast torque response, reduced dependence on machine parameter variations, and a simpler implementation due to the absence of coordinate transformations and current control loops. However, DTC suffers from significant drawbacks: high switching frequency, considerable torque and flux ripples, mechanical vibration and noise, and poor control performance in low-speed operating ranges [4]-[7]. field-oriented control (FOC), in contrast to DTC, offers fast torque response, a wide speed control range, and high efficiency across varying load conditions, achieved by decoupling torque and flux control. Problems related to torque and flux ripples, noise, mechanical vibration, and low-speed operation do not appear in FOC. FOC's main disadvantages are its high sensitivity to machine parameter variations and its significant complexity, stemming from the need for coordinate transformations and multiple control variables. The traditional FOC implementations using proportional-integral (PI) controllers with fixed coefficients often fail to meet the stringent quality demands of high-performance drives [8]-[10].

Modern and intelligent control techniques have been proposed to address these problems [11]-[16]. Among them, sliding mode (SM) control is one of the most prominent methods. It has been widely used in many industrial applications due to its robustness against disturbances, relative simplicity, and ease of tuning and implementation [14]-[16]. However, the major disadvantage of conventional SM control is the chattering phenomenon. Several methods have been proposed to eliminate or alleviate this unwanted effect. Effective approaches include employing higher-order sliding mode (HOSM) control techniques [17]. Quasi-continuous third-order sliding mode (QCTOSM) control is an advanced version of HOSM control designed to mitigate chattering while preserving robustness.

To date, significant research has been conducted on HOSM control [18], [19]. However, many of these studies operate under the assumption that nonlinear systems are primarily affected by general, bounded disturbances. In reality, numerous nonlinear industrial processes (mechanical, robotics, and power distribution) are disturbances can be harmonic signals, the diode rectifiers, and power converters can be considered as a generator of these non-desired harmonic currents [20], Cogging torque, that caused by the misalignment between stator and rotor is the important periodic disturbances affects rotating mechanical machines [21]. Or the periodic disturbances that appear due to the eccentricity of the track in the hard disk drives [22], due to the interaction between the rigid hub and flexible appendage during attitude maneuvering in spacecraft [23]. Therefore, the major challenge of nonlinear drives in the presence of periodic disturbances is the design of an accurate control ensuring good tracking and disturbance rejection performances.

Effective harmonic disturbance cancellation is crucial for many control applications, particularly in drive systems. Several strategies exist, often depending on the available system knowledge. If both the system model and disturbance frequency are precisely known, the internal model principle (IMP) allows for effective feedback compensation [24]. If only the system model is known, a disturbance observer (DO) can be employed to estimate the harmonic disturbance [25]. When the system model is uncertain or unavailable, adaptive control techniques [26] or feedforward methods [27] become relevant. Adaptive control methods based on feedback can also be proposed to tackle known and unknown disturbance frequencies [28], [29]. However, it generally requires some extra information and structural assumptions regarding the system. Harmonic disturbances present in the system can also be identified, characterized, and mitigated using the active disturbance rejection control (ADRC) framework. In this technique, total disturbance of the system consists of all the uncertain elements, seen from the plant perspective as an input-additive. With ADRC, the detailed analytical representation of the system is not required for control synthesis; it prioritizes the issue of aggregated disturbance influence on the controlled output is continuously mitigated. The control design can be achieved through online reconstruction of the total disturbance by means of a specialized observer. The effectiveness of ADRC has been verified in numerous process and motion applications [29], [30]. The result [31], ADRC was applied to compensate for the harmonic disturbance, combining these disturbance rejection strategies with disturbance observers and compensation is required to give a good disturbance cancellation efficiency, but this makes the control system more complex [31], [32].

In contrast to the above solutions, [33] develops a unique disturbance rejection scheme for highly uncertain systems subjected to harmonic disturbances with unknown/known frequencies. Repetitive control (RC) was proven to be an effective tool to reject disturbance and enhance the control performance through its repeated learning process. However, it faces the stability problem and the inability to consider certain characteristics of processes [33], [34]. To overcome these, much research focuses on improving the RC design for non-linear systems [35]-[37]. Especially, a modified RC based on disturbance observer (MRC) was developed to ensure the high-frequency stability and low-frequency periodic disturbances resistance ability of the control strategy. A robust plug-in RC with phase compensation was proposed in [35]. Another approach that the combination of RC with SM, an IIR low-pass filter was applied inside the internal model of RC to improve the stability robustness, is developed in [36]. The article [37], a multi-model identification in presence of the periodic disturbance with an adaptive filter is used to decouple the disturbance and a discrete repetitive sliding mode multi-control are developed to deal the problem of stability of the systems, the

proposed control technique in [37] also combined multi-model SM control with RC to enhance the control performances of nonlinear systems. A disturbance rejection repetitive second-order sliding mode (DRRISOSM) control scheme using improved sliding mode control (ISOSM) technique combined with RC is developed [38]. The improvement in [38] provides superior control and disturbance rejection capability. However, ISOSM with constant gain of STA offers non-adaptive control authority. These gains are a compromise; they can be too low for fast convergence when far from the surface, or unnecessarily high (risking chattering/high control effort) when near the surface. Performance might be less consistent across varying operating conditions compared to a well-designed variable gain scheme. In this paper, to thoroughly solve the problems of periodic harmonic disturbance and accurately track high-performance DSIM drives, a new improved sliding mode control method is proposed.

The main contributions are summarized as follows: i) The proposed control employs an improved variable-gain quasi-continuous third-order sliding mode (VGQSTOSM) provides a smoother control tool compared to SOSM. This potentially leads to ultra-low torque ripple and minimal vibration, offers superior chattering suppression compared to SOSM, and higher precision. Furthermore, by making the gain dependent on the magnitude of the sliding variable, this proposal aims to be adaptive. It provides higher gain when far from the sliding surface (is large), leading to faster convergence and lower gain when close to the sliding surface (is small), potentially reducing chattering further and decreasing control effort near the equilibrium. The robustness of the proposed controller is improved because the adaptive gain mechanism effectively compensates for uncertainties or extended and periodic load disturbances. ii) To specifically improve harmonic disturbance rejection in FOC-based DSIM drives, a load torque disturbance estimator for disturbance identification and a plug-in RC combined with the VGQSTOSM structure are proposed to reject the periodic disturbance. Moreover, the system stability of the system was assured by the virtual control vectors output of speed and current control loops is chosen based on Lyapunov theory.

This paper consists of four parts: i) The mathematical model of the DSIM drive is given in section 2; ii) Section 3 is devoted to the development of a new discrete repetitive sliding model controller; iii) Simulation results are presented in section 4; and v) Section 5 concludes.

## 2. MODEL OF DSIM DRIVE

A DSIM drive system consists of a DSIM fed by a six-phase voltage source inverter (SPVSI) and a DC link, as shown in Figure 1. In this configuration, the SPVSI acts as the primary power converter, delivering the appropriate voltage and frequency required for the DSIM to operate efficiently. Meanwhile, the DC link serves as an energy buffer, helping to maintain voltage stability and enabling the inverter to provide dynamic and responsive control of the motor.

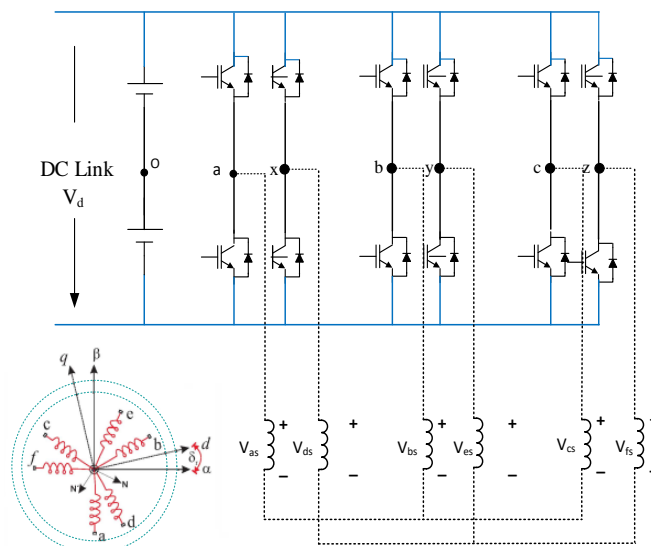


Figure 1. A DSIM drive general diagram

The vector space decomposition (VSD) technique was applied to transform the original six-dimensional space of the machine into three two-dimensional orthogonal subspaces in the stationary reference frame ( $DQ$ ), ( $x - y$ ) and ( $z1 - z2$ ) through a transformation matrix  $6 \times 6$  in (1). Some basic

assumptions have been made to develop the DSIM model. The windings are assumed to be sinusoidally distributed: The magnetic saturation, the mutual leakage inductances, and the core losses are neglected.

$$T_6 = \frac{1}{3} \begin{bmatrix} 1 & \frac{\sqrt{3}}{2} & -\frac{1}{2} & -\frac{\sqrt{3}}{2} & -\frac{1}{2} & 0 \\ 0 & \frac{1}{2} & \frac{\sqrt{3}}{2} & \frac{1}{2} & -\frac{\sqrt{3}}{2} & -1 \\ 1 & -\frac{\sqrt{3}}{2} & -\frac{1}{2} & \frac{\sqrt{3}}{2} & -\frac{1}{2} & 0 \\ 0 & \frac{1}{2} & -\frac{\sqrt{3}}{2} & \frac{1}{2} & \frac{\sqrt{3}}{2} & -1 \\ 1 & 0 & 1 & 0 & 1 & 0 \\ 0 & 1 & 0 & 1 & 0 & 1 \end{bmatrix} \quad (1)$$

The electrical matrix equations in the stationary reference frame for the stator and the rotor may be written as (2):

$$\begin{aligned} [V_s] &= [R_s][I_s] + p([L_s][I_s] + [L_m][I_r]) \\ 0 &= [R_r][I_r] + p([L_r][I_r] + [L_m][I_s]) \end{aligned} \quad (2)$$

where:  $[V]$ ,  $[I]$ ,  $[R]$ ,  $[L]$ , and  $[L_m]$  are voltage, current, resistance, self, and mutual inductance vectors, respectively.  $p$  is the differential operator. Subscripts r and s are related to the rotor and stator resistance, respectively. Since the rotor is a squirrel cage,  $[V]$  is equal to zero. The electromechanical energy conversion only takes place in the only takes place in  $D$ - $Q$  subspace, and the other subspaces just produce losses. Therefore, the control is based on determining the applied voltage in the  $DQ$  reference frame. With this transformation, the DSIM control technique like a classical three-phase IM FOC. The moment equation when expressed, is as (3):

$$T_e = 3P(\psi_{rQ}i_{rD} - \psi_{rD}i_{rQ}) \quad (3)$$

where:  $T_e$ ,  $P$ ,  $\Psi_{rD}$ ,  $\Psi_{rQ}$ ,  $i_{rD}$ ,  $i_{rQ}$  are the electromagnetic torque, number of pole pairs, the rotor flux, and the rotor current, respectively. Like AC drives, motor control in a static reference frame is difficult; therefore, the transformation of the DSIM model to dq rotating reference frame is necessary by using a transformation matrix:

$$T_{dq} = \begin{bmatrix} \cos(\delta) & -\sin(\delta) \\ \sin(\delta) & \cos(\delta) \end{bmatrix} \quad (4)$$

where  $\delta$  is the rotor angular position referred to the stator.

In FOC, the rotor flux and torque are controlled by the  $i_{sd}$  and  $i_{sq}$  components. We have:  $\psi_{rq} = 0$ ;  $\psi_{rd} = \psi_{rd}$ . The space vector differential equations describe the model motor dynamics as (5) and (6).

$$\begin{cases} \frac{d\omega_r}{dt} = \frac{3}{2}P \frac{\delta\sigma L_s}{J} (\psi_{rd}i_{sq}) - \frac{T_L}{J} - B'\omega_r \\ \frac{d\psi_{rd}}{dt} = \frac{L_m}{\tau_r} i_{sd} - \frac{1}{\tau_r} \psi_{rd} \\ L_s \frac{di_{sq}}{dt} = -a i_{sq} + L_s \omega_e i_{sd} + b_r \omega_e \psi_{rd} + c u_{sq} \\ L_s \frac{di_{sd}}{dt} = -a i_{sd} + L_s \omega_e i_{sq} + b_r \omega_e \psi_{rd} + c u_{sd} \end{cases} \quad (5)$$

$$\text{where: } \sigma = 1 - \frac{L_m^2}{L_s L_r}; \delta = \frac{L_m}{\sigma L_s L_r}; a = \frac{L_m^2 R_r + L_r^2 R_s}{\sigma L_r^2}; b = \frac{L_m^2 R_r}{\sigma L_r^2}; c = \frac{1}{\sigma}; \tau_r = \frac{L_r}{R_r}; B' = \frac{B}{J} \quad (6)$$

$u_{sd}$ ,  $u_{sq}$ ;  $i_{sd}$ ,  $i_{sq}$ : The components of inductance;  $e$  and stator current, respectively;  $\psi_{rd}$ ,  $\psi_{rq}$ : Rotor flux components;  $T_e$ ,  $T_L$ : Electromagnetic and load torque;  $d$ - $q$ : Synchronous and stationary axis reference frame quantities, respectively;  $\omega_r$ : the angular velocity (mechanical speed),  $\omega_r = (2/P)\omega_{re}$ ;  $\omega_{re}$ ,  $\omega_{sl}$ ,  $\omega_e$ : the electrical speed respectively Rotor and slip angular and synchronous angular velocity;  $L_s$ ,  $L_r$ : Stator and rotor inductances;  $L_m$ : Mutual inductance;  $R_s$ ,  $R_r$ : Stator and rotor resistances;  $J$ : the inertia of motor and load;  $\sigma$ : Total linkage coefficient;  $B$ : Friction coefficient;  $\tau_r$ : Rotor and stator time constant. The electromagnetic torque and the slip frequency can be expressed in  $dq$  reference frame:

$$T_e = \frac{3P}{2} \frac{L_m}{L_r} \psi_{rd} i_{sq}; \quad \omega_{sl} = \frac{M=L_m}{L_r} \psi_{rd} i_{sq} \quad (7)$$

### 3. DRVGSTAHOSM STRUCTURE FOR FOC OF SPIM DRIVES

#### 3.1. Design the outer speed and flux loop

The classic SM provides high-accuracy solutions and is robust for a wide range of control problems under uncertainty conditions. However, the main restriction of this control method is that high-frequency control switching may easily cause unacceptable practical complications (chattering effect) [39]-[41]. To overcome this problem, in the proposed controller, we propose using an improved order second sliding technique, which is developed based on [39]. The second order slip surfaces according to the rotor flux, speed components are defined as (8):

$$S_m(k) = \begin{bmatrix} s_1(k) \\ s_2(k) \end{bmatrix} = \begin{bmatrix} \varepsilon_{\psi_{rd}} + \lambda_{4.} |\varepsilon_{\psi_{rd}}|^{1/2} \text{sat}(\varepsilon_{\psi_{rd}}) \\ \varepsilon_{\omega_r} + \lambda_{3.} |\varepsilon_{\omega_r}|^{1/2} \text{sat}(\varepsilon_{\omega_r}) \end{bmatrix} \quad (8)$$

where:  $\lambda_{1,2}$  are positive coefficients. The rotor flux, speed are defined as (9).

$$\begin{cases} \varepsilon_{\psi_{rd}} = \psi_{rd}^* - \psi_{rd} \\ \varepsilon_{\omega_r} = \omega_r^* - \omega_r \end{cases} \quad (9)$$

In the presence of periodic disturbances, the second-order sliding mode control performance decreases considerably. To deal with this problem, a combination of repetitive control with improved SOSM control is developed based on [37], [39]. We suppose that the disturbance vector  $d_m(k)$  is periodic with the period  $N$

$$d_m(k) = \begin{bmatrix} d_1(k) \\ d_2(k) \end{bmatrix} = \begin{bmatrix} d_1(k-N) \\ d_2(k-N) \end{bmatrix} = d_m(k-N) \quad (10)$$

Based on the condition of disturbance rejection [38], the sliding functions vector is then given as (11):

$$S_m(k+1) = \phi S_m(k) + \begin{bmatrix} \mu_1 \text{sat}(s_1(k)) \\ \mu_2 \text{sat}(s_2(k)) \end{bmatrix} + \gamma [d_m(k) - d_m(k-N)] \quad (11)$$

where:  $\mu_{1,2}$  are positive coefficients. The control expression of the new system [38] is (12):

$$[u(k)] = [u_m(k) + [u_m^{dis}(k)]] \quad (12)$$

where: vector  $[u_m(k)]$  are designed based on improved quasi-continuous three-order sliding-mode controllers combine variable gain quasi-continuous third order sliding mode (VGQSTOSM) [38]-[41], and they are defined as (13):

$$[u_m(k)] = \begin{bmatrix} u_1(k) \\ u_2(k) \end{bmatrix} = \begin{bmatrix} k_1(t, \varepsilon_{\psi_{rd}}) \frac{\ddot{s}_1 + 2(\dot{s}_1 + |s_1|^{2/3} \text{sat}(|s_1|))(|\dot{s}_1| + |s_1|^{2/3})^{-1/2}}{|\dot{s}_1| + 2(|\dot{s}_1| + |s_1|^{2/3})^{1/2}} \\ k_2(t, \varepsilon_{\omega_r}) \frac{\ddot{s}_2 + 2(\dot{s}_2 + |s_2|^{2/3} \text{sat}(|s_2|))(|\dot{s}_2| + |s_2|^{2/3})^{-1/2}}{|\dot{s}_2| + 2(|\dot{s}_2| + |s_2|^{2/3})^{1/2}} \end{bmatrix} \quad (13)$$

where:

$$\begin{aligned} k_1(t, \varepsilon_{\psi_{rd}}) &= \frac{1}{2} \text{sat}(|s_1|) + \frac{3}{2} k_a |s_1|^{1/2} \text{sat}(|s_1|) + k_a^2 |s_1|; \\ k_2(t, \varepsilon_{\omega_r}) &= \frac{1}{2} \text{sat}(|s_2|) + \frac{3}{2} k_b |s_2|^{1/2} \text{sat}(|s_2|) + k_b^2 |s_2|; \quad \text{with } k_a, k_b > 0 \end{aligned}$$

$[u_m^{dis}(k)]$  are the disturbance vectors be given the system to cancel periodic disturbances and they are defined:

$$[u_m^{dis}(k)] = \begin{bmatrix} u_1^{dis}(k) \\ u_2^{dis}(k) \end{bmatrix} = \begin{bmatrix} \varepsilon_{\psi_{rd}}(k) + \gamma_1 \text{sat}(s_1(k+1)) \\ \varepsilon_{\omega_r}(k) + \gamma_2 \text{sat}(s_2(k+1)) \end{bmatrix} \quad (14)$$

where:  $\gamma_{1,2,3,4}$  are positive coefficients. Lyapunov functions are chosen:

$$V = \frac{1}{2}[V_1^2 + V_2^2] = \frac{1}{2}[s_1(k)^2 + s_2(k)^2] \quad (15)$$

Differentiating both sides in (15), we get (16) and (17).

$$\frac{dV}{dt} = \left[ s_1(k) \frac{ds_1(k)}{dt} + s_2(k) \frac{ds_2(k)}{dt} \right] \quad (16)$$

$$\begin{cases} \frac{ds_1(k)}{dt} = \frac{d[\varepsilon_{\psi rd} + \lambda_1 \cdot |\varepsilon_{\psi rd}|^{1/2} \text{sat}(\varepsilon_{\psi rd})]}{dt} \\ \frac{ds_2(k)}{dt} = \frac{d[\varepsilon_{\omega r} + \lambda_2 \cdot |\varepsilon_{\omega r}|^{1/2} \text{sat}(\varepsilon_{\omega r})]}{dt} \end{cases} \Rightarrow \begin{cases} \frac{ds_1(k)}{dt} = \frac{d[\psi_{rd}^* - \psi_{rd}]}{dt} + \frac{d[\lambda_1 \cdot |\varepsilon_{\psi rd}|^{1/2} \text{sat}(\varepsilon_{\psi rd})]}{dt} \\ \frac{ds_2(k)}{dt} = \frac{d[\omega_r^* - \omega_r]}{dt} + \frac{d[\lambda_2 \cdot |\varepsilon_{\omega r}|^{1/2} \text{sat}(\varepsilon_{\omega r})]}{dt} \end{cases} \quad (17)$$

On the other hand, to satisfy the stability condition according to Lyapunov theory, the sliding surface differential function is chosen as (18).

$$\frac{ds_m(k)}{dt} = -[u_m(k) + u_m^{dis}(k)] \quad (18)$$

Combining (16)-(18),  $i_{sd}^*$ ,  $i_{sq}^*$  virtual vectors are chosen for the outer speed and flux loop:

$$\begin{cases} i_{sd}^*(k) = \frac{\tau_r}{L_m} \left\{ \frac{d\psi_{rd}^*}{dt} + \frac{1}{\tau_r} \psi_{rd} + \frac{d[\lambda_1 \cdot |\varepsilon_{\psi rd}|^{1/2} \text{sat}(\varepsilon_{\psi rd})]}{dt} + [u_1(k) + u_1^{dis}(k)] \right\} \\ i_{sq}^*(k) = \frac{1}{k_{sq} \psi_{rd}} \left\{ \frac{d\omega_r^*}{dt} + \frac{T_L}{J} + B' \omega_r + \frac{d[\lambda_2 \cdot |\varepsilon_{\omega r}|^{1/2} \text{sat}(\varepsilon_{\omega r})]}{dt} + [u_2(k) + u_2^{dis}(k)] \right\} \end{cases} \quad (19)$$

In (19),  $i_{sd}^*$  and  $i_{sq}^*$  virtual control vectors are chosen to satisfy the control objectives, and they are the reference inputs for calculating  $u_{sd}^*$ ,  $u_{sq}^*$  virtual control vectors.  $\Psi_{rd}$  rotor flux is identified by the current model. The load torque  $T_L$  is estimated:

$$\hat{T}_L = \frac{1}{1+\tau_0 p} \left[ \left( \frac{3}{2} \right) P \frac{L_m}{L_r} \psi_{rd} \hat{i}_{sq} - \frac{J}{P} \frac{d\omega}{dt} \right] \quad (20)$$

where:  $\tau_0$  is time gain; and  $p$  is differential.

### 3.2. Design the inner current loop controls

The improved nonlinear slip surface according to the current components is defined as (21):

$$S_m(k) = \begin{bmatrix} s_3(k) \\ s_4(k) \end{bmatrix} = \begin{bmatrix} \varepsilon_{isd} + \lambda_{1\cdot} |\varepsilon_{isd}|^{1/2} \text{sat}(\varepsilon_{isd}) \\ \varepsilon_{isq} + \lambda_{2\cdot} |\varepsilon_{isq}|^{1/2} \text{sat}(\varepsilon_{isq}) \end{bmatrix} \quad (21)$$

where:  $\lambda_{3,4}$  are positive coefficients. The stator current errors are defined in (22).

$$\begin{cases} \varepsilon_{isd} = i_{sd}^* - i_{sd} \\ \varepsilon_{isq} = i_{sq}^* - i_{sq} \end{cases} \quad (22)$$

We suppose that the disturbance vector  $d_m(k)$  is periodic with the period  $N$ .

$$d_m(k) = \begin{bmatrix} d_3(k) \\ d_4(k) \end{bmatrix} = \begin{bmatrix} d_3(k-N) \\ d_4(k-N) \end{bmatrix} = d_m(k-N) \quad (23)$$

Based on the condition of disturbance rejection [51], the sliding functions vector is then given as follows:

$$S_m(k+1) = \phi S_m(k) + \begin{bmatrix} \mu_3 \text{sat}(s_3(k)) \\ \mu_4 \text{sat}(s_4(k)) \end{bmatrix} + \gamma [d_m(k) - d_m(k-N)] \quad (24)$$

where:  $\mu_{3,4}$  are positive coefficients. The control expression of the new system is (25):

$$[u(k)] = [u_m(k) + u_m^{dis}(k)] \quad (25)$$

where: vector  $[u_m(k)]$  are designed based on quasi-continuous three-order sliding-mode controllers [8] combining VGQSTOSM [38]-[41], and they are defined as (26):

$$[u_m(k)] = \begin{bmatrix} u_3(k) \\ u_4(k) \end{bmatrix} = \begin{bmatrix} k_3(t, \varepsilon_{isd}) \frac{\ddot{s}_3 + 2(\dot{s}_3 + |s_3|^{2/3} \text{sat}(s_3))(|\dot{s}_3| + |s_3|^{2/3})^{-1/2}}{|\dot{s}_3| + 2(|\dot{s}_3| + |s_3|^{2/3})^{1/2}} \\ k_4(t, \varepsilon_{isd}) \frac{\ddot{s}_4 + 2(\dot{s}_4 + |s_4|^{2/3} \text{sat}(s_4))(|\dot{s}_4| + |s_4|^{2/3})^{-1/2}}{|\dot{s}_4| + 2(|\dot{s}_4| + |s_4|^{2/3})^{1/2}} \end{bmatrix} \quad (26)$$

where:

$$k_3(t, \varepsilon_{isd}) = \frac{1}{2} \text{sat}(|s_3|) + \frac{3}{2} k_c |s_3|^{1/2} \text{sat}(|s_1|) + k_d^2 |s_3|; \\ k_4(t, \varepsilon_{isd}) = \frac{1}{2} \text{sat}(|s_4|) + \frac{3}{2} k_d |s_2|^{1/2} \text{sat}(|s_1|) + k_d^2 |s_2|; \quad \text{with } k_c, k_d > 0$$

$[u_m^{dis}(k)]$  are the disturbance vectors be given the system to cancel periodic disturbances and they are defined in (27):

$$[u_m^{dis}(k)] = \begin{bmatrix} u_3^{dis}(k) \\ u_4^{dis}(k) \end{bmatrix} = \begin{bmatrix} \varepsilon_{isd}(k) + \gamma_3 \text{sat}(s_3(k+1)) \\ \varepsilon_{isd}(k) + \gamma_4 \text{sat}(s_4(k+1)) \end{bmatrix} \quad (27)$$

where:  $\gamma_{1,2,3,4}$  are positive coefficients. Lyapunov functions are chosen:

$$V = \frac{1}{2} [V_3^2 + V_4^2] = \frac{1}{2} [s_3(k)^2 + s_4(k)^2] \quad (28)$$

Differentiate both sides in (15) we get:

$$\frac{dV}{dt} = \left[ s_3(k) \frac{ds_3(k)}{dt} + s_4(k) \frac{ds_4(k)}{dt} \right] \quad (29)$$

$$\begin{cases} \frac{ds_3(k)}{dt} = \frac{d[\varepsilon_{isd} + \lambda_3 |\varepsilon_{isd}|^{1/2} \text{sat}(\varepsilon_{isd})]}{dt} \\ \frac{ds_4(k)}{dt} = \frac{d[\varepsilon_{isd} + \lambda_4 |\varepsilon_{isd}|^{1/2} \text{sat}(\varepsilon_{isd})]}{dt} \end{cases} \Rightarrow \begin{cases} \frac{ds_3(k)}{dt} = \frac{d[i_{sd}^* - i_{sd}]}{dt} + \frac{d[\lambda_3 |\varepsilon_{isd}|^{1/2} \text{sat}(\varepsilon_{isd})]}{dt} \\ \frac{ds_4(k)}{dt} = \frac{d[i_{sq}^* - i_{sq}]}{dt} + \frac{d[\lambda_4 |\varepsilon_{isd}|^{1/2} \text{sat}(\varepsilon_{isd})]}{dt} \end{cases} \quad (30)$$

On the other hand, to satisfy the stability condition according to Lyapunov theory, the sliding surface differential function is chosen as (31).

$$\frac{ds_m(k)}{dt} = -[u_m(k) + u_m^{dis}(k)] \quad (31)$$

Combining expressions in (29) and in (31),  $u_{sd}^*$ ,  $u_{sq}^*$  virtual control vectors are chosen as (32).

$$\begin{cases} u_{sd}^*(k) = \frac{L_s}{c} \left\{ \frac{di_{sd}^*}{dt} + ai_{sd} - L_s \omega_e i_{sq} - b \psi_{rd} + \frac{d[\lambda_3 |\varepsilon_{isd}|^{1/2} \text{sat}(\varepsilon_{isd})]}{dt} + [u_3(k) + u_3^{dis}(k)] \right\} \\ u_{sq}^*(k) = \frac{L_s}{c} \left\{ \frac{di_{sq}^*}{dt} + ai_{sq} - L_s \omega_e i_{sd} - b_r \omega_e \psi_{rd} + \frac{d[\lambda_4 |\varepsilon_{isd}|^{1/2} \text{sat}(\varepsilon_{isd})]}{dt} + [u_4(k) + u_4^{dis}(k)] \right\} \end{cases} \quad (32)$$

where:  $\lambda_{3,4}$ ,  $\mu_{3,4}$ ,  $\gamma_{3,4}$  are positive coefficients

### 3.3. Stability analysis

The Lyapunov function of the system is defined in (15). Taking the differentiation of both sides of the Lyapunov function, we get (16). Combining (16)-(18) we get (33).

$$\frac{dV}{dt} = - \left[ s_1(k) [u_1(k) + u_1^{dis}(k)] + s_2(k) [u_2(k) + u_2^{dis}(k)] + s_3(k) [u_3(k) + u_3^{dis}(k)] + s_4(k) [u_4(k) + u_4^{dis}(k)] \right] \quad (33)$$

From (33) we get:

$$\frac{dv}{dt} < 0 \text{ with } \forall \{\lambda; \gamma; \mu > 0\} \quad (34)$$

Thus, the system is always stable according to Lyapunov stability theory.

#### 4. SIMULINK AND DISCUSSION

The performance of the DRVGQSTOSM controller for FOC of DSIM drives is validated through simulation using MATLAB software. To increase the reliability, comparison frameworks are established, similar surveys are also implemented for SOSM control in [17], DRRISOSM control in [38], these comparison to make clearly the second order sliding mode control shows that then combination RC control and improved HOSM control give a deal has superior performance in terms of harmonic immunity and accurate tracking of the reference speed, the PI controller is also chosen to make the create comparison data because it is now still the standard solution and the most widely used solution in industry and engineering practice. Additionally, DRVGQSTOSM control is also compared with other latest methods in [15], [28], to confirm the effectiveness of the proposed control structure. The block diagram of the SPIM drive system is shown in Figure 2. In these simulations, a six-phase squirrel-cage type IM with the rated parameters is given as follows: 1 HP, 6-phase, 220 V, 50 Hz, 4 poles, 1450 rpm.  $R_s = 10.1 \Omega$ ,  $R_r = 9.8546 \Omega$ ,  $L_s = 0.833457 H$ ,  $L_r = 0.830811 H$ ,  $L_m = 0.783106 H$ , and  $J = 0.0088 \text{ kg.m}^2$ .

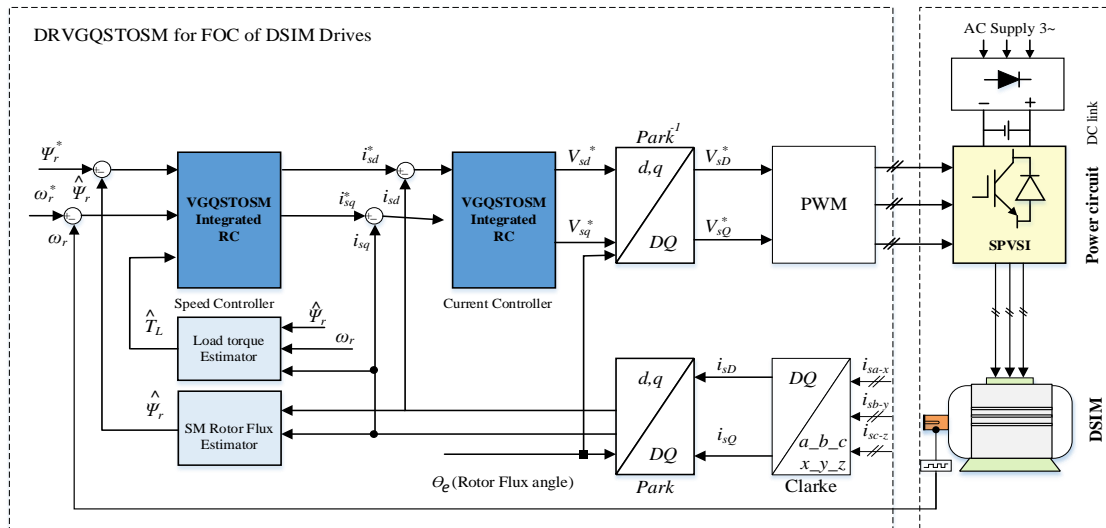


Figure 2. FOC Vector control of DSIM drive using DRVGQSTOSM control structure

##### 4.1. The dynamic performance of the proposed controller under variable speed and torque disturbance

The dynamic performance of the DRVGQSTOSM controller was confirmed through the starting and reversing mode investigation tests. Figure 3 shows the speed, torque, current, and rotor flux responses as the reference speed increases from 0 to 1440 rpm at  $t = 0.5 \text{ s}$ ; then reversed to -1440 rpm then decreased to 0 at  $t = 3.4 \text{ s}$ , respectively, and increased to 100 rpm at  $t = 5.5 \text{ s}$ , rated load applied at  $t = 1.5 \text{ s}$ . This survey was carried out based on the experiments in [16], in which FC combined with the SOSM (FSOSMC) was proposed. This investigation was also carried out with the PI, SOSM control in [18], and DRRISOSM control in [38] to get comparison data.

The results show that the DRVGQSTOSM controller can provide faster dynamic responses and stabilization time. The start-up time from 0 to 1440 rpm in the case of the drive system using PI, SOSM, DRRISOSM, and DRVGQSTOSM controllers is 0.19 s, 0.125 s, 0.105 s, and 0.09 s, respectively. At  $t = 1.5 \text{ s}$ , the rated torque is applied, negatively affecting the performance of the PI controller, causing a sudden speed drop of 29.11 rpm (2.06%) and taking 0.135 s to stabilize. The steady state error (SS error) is 3.89 rpm (0.27%). The load disturbance also impacted the performance of SOSM [18], DRRISOSM [38] controllers, and the proposed DRVGQSTOSM controller, but these control strategies performed quite well; the speed distortions were not too serious due to the load disturbance being identified and put into SOSM, DRRISOSM, and DRVGQSTOSM controllers, which indirectly helps effectively reconstruct the load



disturbance and allows this control faster compensation than PI control. The speed drop of SOSM and DRRISOSM when applying load disturbance is similar at 12.23 rpm (0.849%), 0.011s to stabilize, the SS error is 0.05% (SOSM), and almost zero DRRISOSM. Comparing Simulink results, it is easy to see that DRVGQSTOSM controls the load disturbance better. The transient parameters of the DRVGQSTOSM proposed controller are 5.12 rpm (0.35% drop) speed drop, and 0.003s to stabilize, SS error almost zero. At time  $t = 1.5$ s, the speed is reversed directly from 1440 rpm to -1440 rpm. As soon as the speed reversal is applied, the torque is immediately reversed, the motor starts to decelerate to reach 0 speed, and then accelerates in the opposite direction and stabilizes at -1440 rpm. The total reversal time of the DSIM drive system using PI, SOSM, DRRISOSM, and DR VGQSTOSM controllers is 0.283 s, 0.217 s, 0.188 s, and 0.121 s, respectively. When observing the FSOSMC controller in [15] under variable speed and torque disturbance shown that this strategy also performs the good reversal; however, torque and rotor flux oscillations appear during the survey, and the chattering phenomenon has not been eliminated.

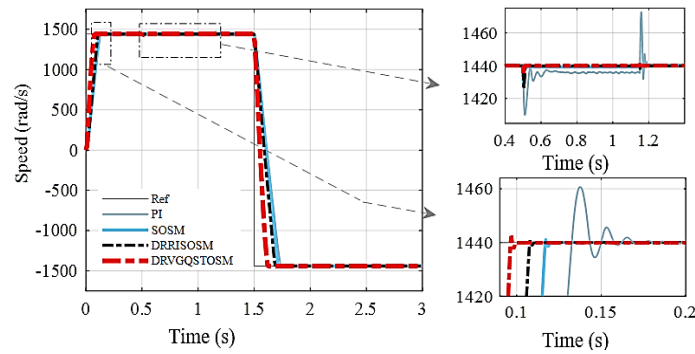


Figure 3. Performance of PI, SOSM, DRRISOSM, and DRVGQSTOSM controllers under reverse speed

As we knew, to deal with the tracking and harmonic disturbance rejection performance and robustness of the controllers, a DRVGQSTOSM control strategy with improved HOSM combined with RC is proposed using the variable (adaptive) gains  $k(t, \varepsilon)$  that are functions of the system's state, specifically adapting based on the magnitude of the  $s$  sliding variables. These gains increase when the system state is far from the sliding surface ( $|s|$  is large) and decrease when the state is close ( $|s|$  is small), making the control effort automatically adjust to the system's proximity. High gain far away promotes fast convergence; low gain nearby reduces chattering. By reducing this gain near the sliding surface, the high-frequency switching (chattering) inherent in SMC can be significantly attenuated. It also helps potentially improve performance, offer a better balance between fast transient response and smooth steady-state behavior, and may use control energy more efficiently by avoiding unnecessarily high gains when the system is already near the target. RC is also integrated into VGQSTOSM to further enhance noise cancellation. It is these things that enable the proposed DRVGQSTOSM controller to provide superior control and disturbance rejection capability.

#### 4.2. Test for robustness against harmonic disturbance

In this part, to validate the robustness of the proposed controller, the first test was performed with a harmonic load disturbance added to the system. Specifically, the test is implemented with the motor load having a significant cogging torque due to the motor and load being coupled by a coupler below, where considerable misalignment appears [28]. The drive system appears to have strong torque harmonic components; the most significant orders are the first, fourth, and 12th. The first and fourth harmonics are present due to the misalignment of the system, and the 12th harmonic is generated by the mutual torque and cogging components of the load, both at the same frequency [28]. In this part, the speed was surveyed at 100 rpm and 600 rpm with an extended harmonics load activated at  $t = 1$  s. The harmonic torque disturbance can be described in terms of the rotor position,  $\theta$ , as:

$$T_d(k) = T_c \cos(m\theta) + T_s \sin(m\theta) \quad (35)$$

where  $T_s$ ,  $T_c$  are the  $m$ th harmonic sine and cosine components. In this case, at 100 and 600 rpm speed, the harmonic frequencies appear 1.66, 6.66, 20 Hz, and at 10, 40, and 120 Hz, respectively, (the first, fourth, and 12th harmonic orders). Figure 4 illustrates the speed and torque responses for PI, SOSM, and the proposed DR VGQSTOSM controllers under these conditions. The results indicate that the PI controller, while

attempting speed regulation, suffers from significant performance degradation due to its fixed gains ( $K_p$ ,  $K_i$ ) and the absence of a torque estimation mechanism. This leads to the largest speed and torque oscillations when harmonic disturbances are present. The SOSM controller performs reasonably well under normal torque disturbances but struggles with harmonic disturbances, exhibiting increased speed and torque oscillations, albeit smaller than those observed with the PI controller. Comparatively, the adaptive feedforward controller (AFC) presented in [28] under harmonic disturbance conditions shows an inability to completely reject all external disturbances. In contrast, the proposed DR VGQSTOSM controller effectively eliminates harmonic effects, ensuring robust and stable operation at both speeds, 100 (shown in Figure 4(a)) and 600 rpm (shown in Figure 4(b)).

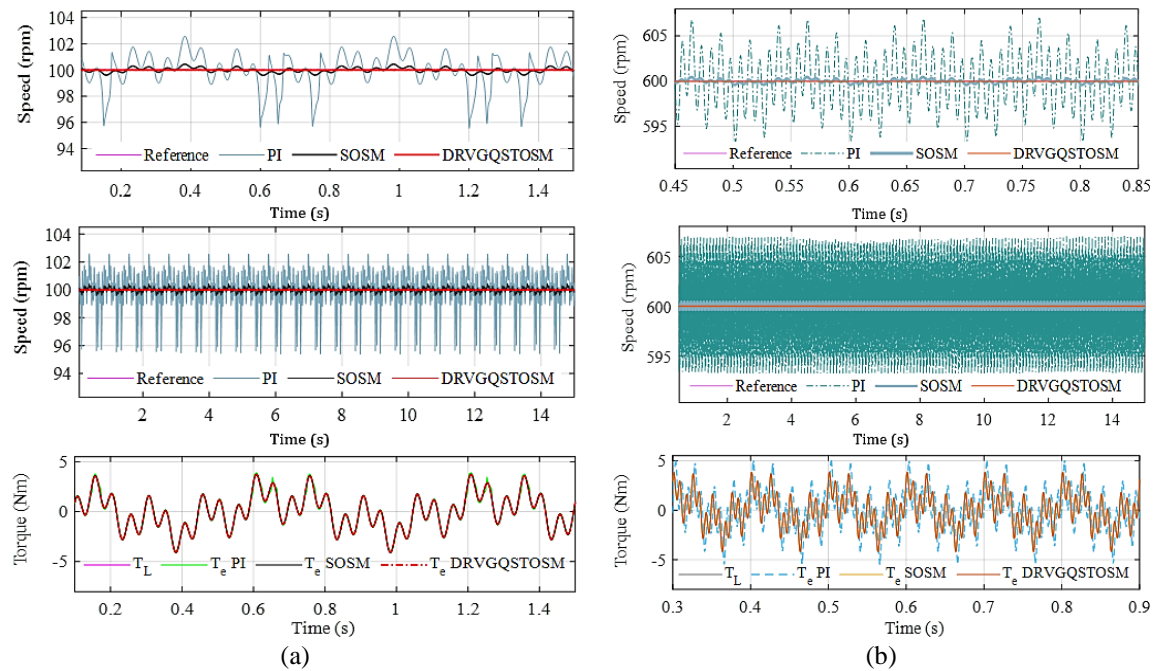


Figure 4. The speed, torque, isq torque current responses of PI, SOSM, DR VGQSTOSM under harmonic torque disturbance at (a) 100 rpm and (b) 600 rpm

A second test to confirm the robustness of the proposed controllers to step load disturbances is conducted, and the speed is kept constant at 1440 rpm. This investigation replicates the test conditions outlined in [25] under step torque disturbance at high speed, load torque is set up:  $T_L = [7, 0, -7, 0, 7]$  Nm at  $t = [0, 0.8, 1.6, 2.1, 3]$  s. The resulting waveforms, shown in Figure 5, show that the PI controller's performance was significantly affected by the load torque disturbances. Observe the subplot (zoom Figure 5) at time  $t = 3$  s when applying a step load disturbance, the PI controller has steady state and transient parameters quite large (speed drop is 25.3 rpm (1.76%), convergence time is 0.07s, steady state error (SS error) is 4.63 rpm (0.32%)). This step load disturbance also impacted the SOSM and DR VGQSTOSM controllers; however, their performance was considerably better than PI controller. Both strategies effectively mitigate speed distortions because the load disturbance is estimated and incorporated into their respective control laws. The inherent robustness of SM control further contributes to effective disturbance reconstruction and faster compensation compared to the PI controller. For SOSM, the drop speed is 9.85 rpm (0.68%), the converge time is 0.0089s, SS error is 1.23 rpm (0.085%). Notably, the DR VGQSTOSM controller, utilizing a combination of an improved high-order sliding mode structure with variable gain and RC, achieved superior dynamic and SS performance compared to the standard SOSM controller, with a drop speed is 5.81 rpm (0.4%), a convergence time is 0.003s, SS error is 0.08 rpm (0.005%).

From the above comparative analyses confirmed that the proposed DRVGQSTOSM scheme offers superior overall control capability. It tracks the reference speed quickly and accurately, and it also demonstrating robustness against load disturbances. When comparing with the results in [17], [28], [38] shown the DRVGQSTOSM controller provides more effective control tools with low steady-state error, reduced torque ripple, and better overall dynamic control performance.

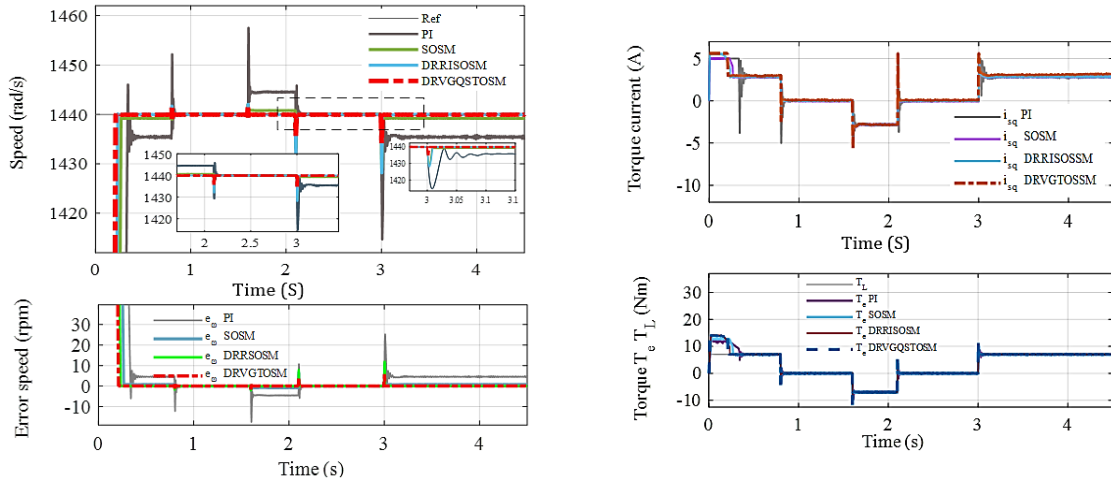


Figure 5. The speed, torque, isq torque current responses of PI, SOSM, DRRISOSM, and DR VGQSTOSM under step torque disturbance at high speed

#### 4.3. Test for robustness against SPIM parametric uncertainties

To more clearly demonstrate the proposed controller's robustness to load disturbances and the impact of DSIM parameter variations, another survey was conducted under load disturbance conditions, the machine parameters  $R_s$ ,  $R_r$  will be increasing to 1.25 and 1.5 times the normal stator and rotor resistance, the speed is keep by constant at low speed (95 rpm), external load step changes of 0 to rated load at 0.2 s, both  $R_s$  and  $R_r$  are increased 25% and 50% at 1s and 1.5 s ( $R_s^*=1.25 R_r$ ,  $R_r^*=1.25 R_s$ ;  $R_s^*=1.5 R_r$ ,  $R_r^*=1.5 R_s$ ) and at  $t=2$  s decreasing to nominal value. Figure 6 shows the speed, rotor flux, and torque responses when parameters  $R_s$ ,  $R_r$  change for the PI and the DRVGQSTOSM controller. At time  $t = 1$  s and  $t = 1.5$  s,  $R_s$ ,  $R_r$  increase; the response of speed, flux, and torque is affected by this change. They are speed decreases and oscillations appear; these oscillations increase when  $R_s$ ,  $R_r$  increase. The results in Figure 6 show that when the variables  $R_s$ ,  $R_r$  with a PI controller appear, the oscillation phenomenon of speed, torque, and flux, the SS error of PI is 9.14% and tends to increase. Opposite, the proposed DRVGQSTOSM schemes have the capability to control the speed very well. It is almost unaffected by this parameter change. The SS error of DRVGQSTOSM does not change and is almost zero.

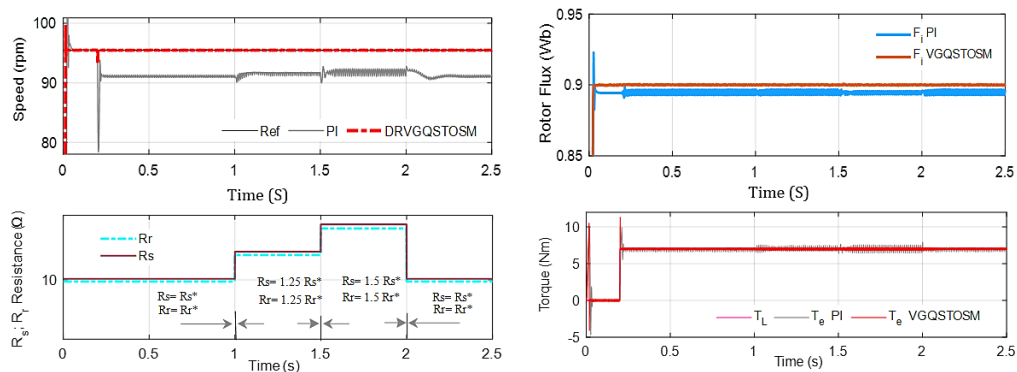


Figure 6. The speed, rotor flux, and torque responses when parameters  $R_s$ ,  $R_r$  change

#### 4.4. Test for robustness against open circuit fault

To confirm the performance and the robustness under open circuit fault at low speed and high speed, two surveys are made at constant speed (100 rpm and 1000 rpm) with rated load torque with open phase fault at  $t = 0.5$  s (phase a opened). Figure 7 and Figure 8 show the performance of the PI, DRRISOSM, and DRVGQSTOSM controllers at low and high speeds. At time  $t = 0.5$  s, phase a of the DSIM is opened, the PI controller is severely affected, causing loss of convergence and stability when the fault. In contrast, because RC improves HOSM in [38] and in DRVGQSTOSM made to both loop control is made, so both these

controllers have superior robustness, stability, and high-speed convergence. In particular, the DRVQSTOSM controller shows the ability to eliminate disturbances, chattering, and fast convergence in the fault case.

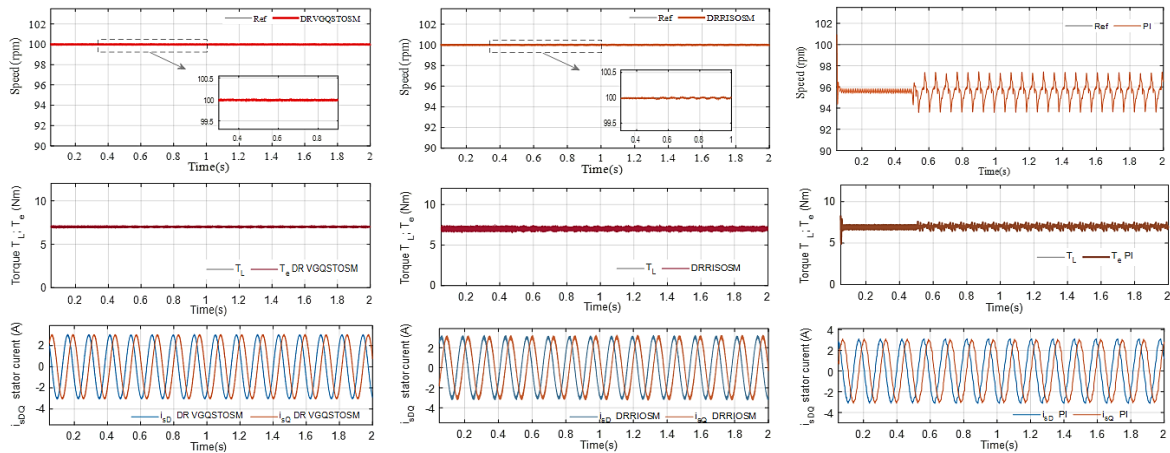


Figure 7. The speed, torque, and rotor flux responses under open phase fault (phase a opened at low speed)

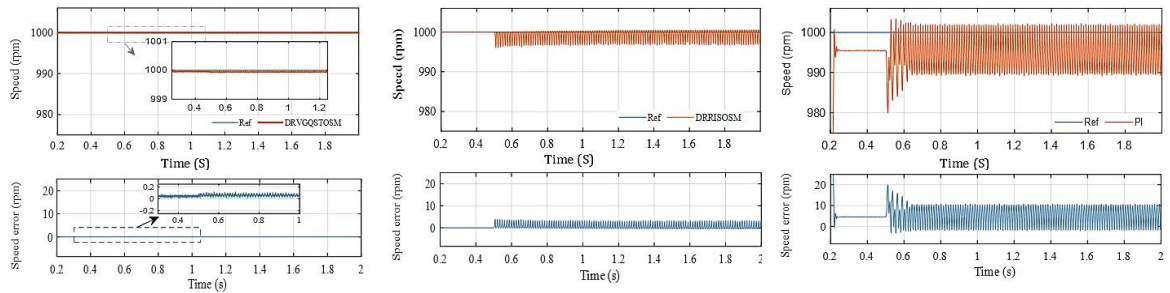


Figure 8. The speed and speed error responses under open phase fault (phase a opened at high speed)

## 5. CONCLUSION

This paper proposes an adaptive DRVQSTOSM control strategy with improved HOSM combined RC. In this proposed VGQSTOSM strategy uses the improved high order (third order) sliding integrated RC and a load torque disturbance estimator help to reduce chattering, cancel the periodic and extended load disturbances effectively. The improved high order third order sliding provides a smoother control tool compared to SOSM, potentially lead to ultra-low torque ripple and minimal vibration, offers superior chattering suppression compared to SOSM, higher precision. Furthermore, the variable (adaptive) gains  $k(t, \varepsilon)$  that are functions of the system's state. These gains will increase when the system state is far from the sliding surface ( $|s|$  is large) and decrease when the state is close ( $|s|$  is small). This makes the control effort automatically adjusts to the system's proximity. High gain far away promotes fast convergence; low gain nearby reduces chattering. By reducing this gain near the sliding surface, the high-frequency switching (chattering) inherent in SMC can be significantly attenuated. It also helps potentially improved performance and offers a better balance between fast transient response and smooth steady-state behavior and may use control energy more efficiently by avoiding unnecessarily high gains when the system is already near the target. Simulation results confirm the reference tracking and periodic disturbance rejection performance, robustness of the proposed controllers for FOC of DSIM drives.

## FUNDING INFORMATION

Authors state no funding involved.

## AUTHOR CONTRIBUTIONS STATEMENT

This journal uses the Contributor Roles Taxonomy (CRediT) to recognize individual author contributions, reduce authorship disputes, and facilitate collaboration.



Name of Author	C	M	So	Va	Fo	I	R	D	O	E	Vi	Su	P	Fu
Ngoc Thuy Pham	✓	✓	✓	✓	✓	✓	✓	✓	✓	✓		✓	✓	
Phu Diep Nguyen		✓	✓	✓	✓	✓		✓	✓	✓	✓	✓		

C : Conceptualization

M : Methodology

So : Software

Va : Validation

Fo : Formal analysis

I : Investigation

R : Resources

D : Data Curation

O : Writing - Original Draft

E : Writing - Review &amp; Editing

Vi : Visualization

Su : Supervision

P : Project administration

Fu : Funding acquisition

## CONFLICT OF INTEREST STATEMENT

Authors state no conflict of interest.

## DATA AVAILABILITY

The data that support the findings of this study are available on request from the corresponding author, [NP], upon reasonable request.

## REFERENCES




- [1] E. Levi, "Multiphase electric machines for variable-speed applications," *IEEE Transactions on Industrial Electronics*, vol. 55, no. 5, pp. 1893–1909, 2008, doi: 10.1109/TIE.2008.918488.
- [2] A. Oumar, "Robust nonlinear controller of the speed for double star induction machine in the presence of a sensor fault," *International Journal of Intelligent Engineering and Systems*, vol. 13, pp. 124–133, 2022.
- [3] G. Sifelislam, T. Bekheira, N. Kamal, N. Mokhtar, and A. Idir, "Virtual vector-based neural network DTC scheme for dynamic performance improvement of dual-star induction motor drive," *Advances in Electrical Engineering, Electronics and Energy*, vol. 11, p. 100938, 2025.
- [4] A. Chantoufi and others, "Direct torque control-based backstepping speed controller of doubly fed induction motors in electric vehicles; experimental validation," *IEEE Access*, vol. 12, pp. 139758–139772, 2024.
- [5] G. Boukhalfa, S. Belkacem, A. Chikhi, and S. Benagoune, "Direct torque control of dual star induction motor using a fuzzy-PSO hybrid approach," *Applied Computing and Informatics*, vol. 18, pp. 74–89, 2022.
- [6] R. Belal, M. Flitti, and M. L. Zegai, "Tuning of PI speed controller in direct torque control of dual star induction motor based on genetic algorithms and neuro-fuzzy scheme," *Revue Roumaine des Sciences Techniques—Série Électrotechnique et Énergétique*, vol. 69, no. 1, pp. 9–14, 2024.
- [7] B. D. Lemma, S. Pradabane, and T. Sutikno, "Improvised direct torque control of a permanent magnet synchronous motor," *International Journal of Power Electronics and Drive Systems*, vol. 15, no. 1, pp. 19–26, 2024.
- [8] S. Benabdallah, Boumediene, and others, "Fuzzy direct field oriented control of a double stator induction motor (DSIM) with an MRAS observer dedicated to photovoltaic pumping system," *Przeglad Elektrotechniczny*, vol. 98, no. 5, 2022.
- [9] A. Das and S. Choudhury, "A novel speed sensor-less stator flux-oriented vector control of dual-stator induction generator for grid-tied wind energy conversion system," *International Journal of Circuit Theory and Applications*, vol. 53, no. 1, pp. 380–408, 2025.
- [10] N. T. Pham and T. D. Le, "A novel FOC vector control structure using RBF tuning PI and SM for SPIM drives," *International Journal of Intelligent Engineering and Systems*, vol. 14, no. 3, pp. 429–440, 2021.
- [11] S. Suganthi and R. Karpagam, "Dynamic performance improvement of PMSM drive using fuzzy-based adaptive control strategy for EV applications," *Journal of Power Electronics*, vol. 23, no. 3, pp. 510–521, 2023.
- [12] C. P. Gor, V. A. Shah, and B. Rangachar, "Fuzzy logic based dynamic performance enhancement of five phase induction motor under arbitrary open phase fault for electric vehicle," *International Journal of Emerging Electric Power Systems*, vol. 22, no. 4, pp. 473–492, 2021.
- [13] A. Abougarair, M. Aburakhis, and Edardar, "Adaptive neural networks based robust output feedback controllers for nonlinear systems," *International Journal of Robotics and Control Systems*, vol. 3, no. 1, pp. 37–56, 2022.
- [14] F. Shiravani, P. Alkorta, J. A. Cortajarena, and O. Barambones, "An enhanced sliding mode speed control for induction motor drives," in *Actuators*, 2022, p. 18, doi: 10.3390/act11010018.
- [15] E. Terfia and others, "Optimal third-order sliding mode controller for dual star induction motor based on grey wolf optimization algorithm," *Heliyon*, vol. 10, no. 12, 2024.
- [16] M. B. Hossen and M. Habibullah, "Performance analysis of a robust MF-PTC strategy for induction motor drive," *International Journal of Power Electronics and Drive Systems*, vol. 15, no. 1, pp. 251–260, 2024.
- [17] N. T. Pham, "Speed tracking of field oriented control SPIM drive using (BS\\_SOSM) nonlinear control structure," *WSEAS Transactions on Systems and Control*, vol. 14, pp. 291–299, 2019.
- [18] J. Qiu, W. Ji, and M. Chadli, "A novel fuzzy output feedback dynamic sliding mode controller design for two-dimensional nonlinear systems," *IEEE Transactions on Fuzzy Systems*, vol. 29, no. 10, pp. 2869–2877, 2021.
- [19] N. T. Pham and T. D. Le, "A Novel Improved VGSTA BS\\_SM control structure for vector control of high performance SPIM drives," *International Journal of Intelligent Engineering and Systems*, vol. 15, no. 1, pp. 155–166, 2022.
- [20] I. Sami, S. Ullah, A. Basit, N. Ullah, and J. S. Ro, "Integral super twisting sliding mode based sensorless predictive torque control of induction motor," *IEEE Access*, vol. 8, pp. 186740–186755, 2020, doi: 10.1109/ACCESS.2020.3028845.
- [21] S. Malo and R. Griño, "Adaptive feed-forward cancellation control of a full-bridge DC-AC voltage inverter," *IFAC Proceedings Volumes*, vol. 41, no. 2, pp. 4571–4576, 2008.
- [22] L. Rosca, "An online observer for minimization of pulsating torque in SMPM motors," *PLOS ONE*, vol. 11, no. 4, 2016.
- [23] C. Zhong, Z. Chen, and Y. Guo, "Attitude control for flexible spacecraft with disturbance rejection," *IEEE Transactions on Aerospace and Electronic Systems*, vol. 53, no. 1, pp. 101–110, 2017.
- [24] H. Xie, Y. Zhang, K. Song, and C. Shao, "Disturbance rejection based engine speed control with rotational inertia online estimation," in *Proceedings of the 2021 40th Chinese Control Conference (CCC)*, Shanghai, China, 2021.

*Paper's should be the fewest possible that accurately describe ... (First Author)*




- [25] E. Shahmoradi and M. Mojiri, "Rejection of sinusoidal disturbance of unknown frequency in linear systems with unknown input delay," in *International Conference on Control, Instrumentation and Automation (ICCIA)*, 2023, pp. 1–6.
- [26] T.-B. Airimitoie, I. D. Landau, R. Melendez, and L. Dugard, "Algorithms for Adaptive feedforward noise attenuation—a unified approach and experimental evaluation," *IEEE Transactions on Control Systems Technology*, vol. 29, no. 5, pp. 1850–1862, 2021.
- [27] J. Stewart and P. Ioannou, "Rejection of sinusoidal disturbances with unknown slowly time-varying frequencies for linear time-invariant systems," *IEEE Transactions on Automatic Control*, vol. 69, no. 8, pp. 5531–5537, Aug. 2024.
- [28] N. Abou-Qamar and C. J. Hatziaioniu, "Cancellation of harmonic torque disturbance in permanent magnet synchronous motor drives by using an adaptive feedforward controller," *IET Power Electronics*, vol. 11, no. 14, pp. 2215–2221, 2018.
- [29] H. S. Ramírez, A. L. Juárez, M. R. Neria, and E. W. Z. Bustamante, *Active disturbance rejection control of dynamic systems: a flatness-based approach*. Butterworth-Heinemann, 2018.
- [30] Y. Yan, J. Yang, Z. Sun, C. Zhang, S. Li, and H. Yu, "Robust speed regulation for PMSM servo system with multiple sources of disturbances via an augmented disturbance observer," *IEEE/ASME Transactions on Mechatronics*, vol. 23, no. 2, pp. 769–780, 2018.
- [31] M. R. Stankovic, R. Madonski, S. Shao, and D. Mikluc, "On dealing with harmonic uncertainties in the class of active disturbance rejection controllers," *International Journal of Control*, vol. 0, no. 0, pp. 1–16, 2020.
- [32] Z. Yin, C. Bai, N. Du, C. Du, and J. Liu, "Research on internal model control of induction motors based on Luenberger disturbance observer," *IEEE Transactions on Industrial Electronics*, vol. 36, no. 7, pp. 8155–8170, 2021.
- [33] Y. H. Lan, J. Y. Wu, and J. H. She, "Optimal sliding mode preview repetitive control for continuous-time nonlinear systems," *International Journal of Control*, vol. 96, no. 10, pp. 2415–2424, 2023.
- [34] M. Tian, B. Wang, Y. Yu, Q. Dong, and D. Xu, "Discrete-time repetitive control-based ADRC for current loop disturbances suppression of PMSM Drives," *IEEE Transactions on Industrial Informatics*, vol. 18, no. 5, pp. 3138–3149, 2022, doi: 10.1109/TII.2021.3107635.
- [35] Q. Zhang, H. Guo, Y. Liu, C. Guo, and J. Sun, "Robust plugin repetitive control for speed smoothness of cascaded-PI PMSM drive," *Mechanical Systems and Signal Processing*, vol. 163, no. 8, 2021.
- [36] M. Zhu, Y. Ye, Y. Xiong, and Q. Zhao, "Parameter robustness improvement for repetitive control in grid-tied inverters using IIR filter," *IEEE Transactions on Power Electronics*, vol. 36, no. 7, pp. 8454–8463, 2021.
- [37] K. Dehri, A. Messaoud, and R. Ben Abdenour, "A discrete repetitive sliding mode multicontrol for non-linear systems," *International Journal of Systems Science*, 2021, doi: 10.1080/00207721.2020.1870017.
- [38] N. T. Pham and T. D. Le, "Disturbance Rejective Repetitive\Improved Second Order Sliding Mode Control for High Performance SPIM Drives," *International Journal of Intelligent Engineering and Systems*, vol. 17, no. 6, pp. 1163–1178, 2024.
- [39] J. Derbel, Q. Ghommam, and Q. Zhu, *Applications of Sliding Mode Control*. Springer, 2017.
- [40] Y. Shtessel, C. Edwards, L. Fridman, and A. Levant, *Sliding Mode Control and Observation*. Springer, 2010.
- [41] L. Fridman and J.-P. Barbot, *Recent Trends in Sliding Mode Control*. The Institution of Engineering and Technology, 2016.

## BIOGRAPHIES OF AUTHORS



**Ngoc Thuy Pham**    is a lecturer in the Department of Electrical Engineering Technology, Industrial University of Ho Chi Minh City (IUH), Ho Chi Minh, Viet Nam. She received the B.Sc. and M.Sc. degrees in Electrical Engineering from Thai Nguyen University of Technology in 1994 and Ho Chi Minh City University of Technology (HCMUT) in 2009, respectively, and a Ph.D. degree in control engineering and automation from TE and Electrical Engineering from Ho Chi Minh City University of Transport, in 2020. Her current research interests include power electronics, AC motor drives, intelligent control, multiphase induction motor, sensorless control of multiphase induction motor drives, and embedded systems. She can be contacted at email: phamthuyngoc@iuh.edu.vn or ngocpham1020@gmail.com.



**Phu Diep Nguyen**    was born in 1993 in Vietnam. He received his engineer's degree in Electrical and Electronic Engineering from Ho Chi Minh City University of Industry in 2015 and subsequently worked for the Ho Chi Minh City Oil and Gas Single-Member Limited Liability Company. In 2024, he began pursuing the Master's program at Ho Chi Minh City University of Industry. His research interests include motor drives, multiphase motors, renewable energy, embedded systems, and intelligent control. He can be contacted at email: phudiep.tradin@gmail.com or diepnp2431@pgr.iuh.edu.vn.